JCTC Journal of Chemical Theory and Computation

Article

pubs.acs.org/JCTC

Free Energy Calculations for the Peripheral Binding of Proteins/Peptides to an Anionic Membrane. 1. Implicit Membrane Models

Leili Zhang, Arun Yethiraj, and Qiang Cui*

Department of Chemistry and Theoretical Chemistry Institute, University of Wisconsin-Madison, 1101 University Avenue, Madison, Wisconsin 53706, United States

Supporting Information

ABSTRACT: The binding of peptides and proteins to the surface of complex lipid membranes is important in many biological processes such as cell signaling and membrane remodeling. Computational studies can aid experiments by identifying physical interactions and structural motifs that determine the binding affinity and specificity. However, previous studies focused on either qualitative behaviors of protein/membrane interactions or the binding affinity of small peptides. Motivated by this observation, we set out to develop computational protocols for bimolecular binding to charged membranes that are applicable to both peptides and large proteins. In this work, we explore a method based on an implicit membrane/solvent model (generalized Born with a simple switching in combination with the Gouy−Chapman−Stern model for a charged interface), which we expect to lead to useful results when the binding does not implicate significant membrane deformation and local demixing of lipids. We show that the binding free energy can be efficiently computed following a thermodynamic cycle similar to protein−ligand binding calculations, especially when a Bennett acceptance ratio based protocol is used to consider both the membrane bound and solution conformational ensembles. Test calculations on a series of peptides show that our computational approach leads to binding affinities in encouraging agreement with experimental data, including for the challenging example of the bringing of flexible MARCKS-ED peptides to membranes. The calculations highlight that for a membrane with a significant fraction of anionic lipids, it is essential to include the effect of ion adsorption using the Stern model, which significantly modifies the effective surface charge. This implicit membrane model based computational protocol helps lay the groundwork for more systematic analysis of protein/peptide binding to membranes of complex shape and composition.

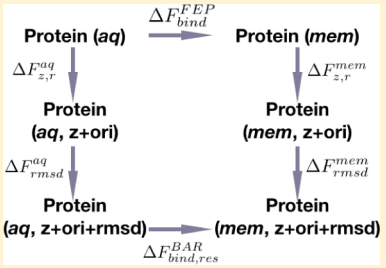

INTRODUCTION

The interaction between proteins/peptides and lipid membranes is involved in many fundamental cellular processes such as protein localization, signaling, and cell−cell adhesion.[1−4] Lipid membranes in many organelles undergo constant remodeling during processes such as exo/endocytosis and the formation of pseudo-organelles such as chromatophores in photosynthetic bacteria; many elementary steps in these processes are driven by protein/membrane interactions.[5−8] In another example, although the *in vivo* mechanisms of antimicrobial peptides/polymers remain actively debated,[9,10] their action starts with preferential binding to specific bacterial cell membranes.[11,12] Finally, an engineering motivated example involves designing peptides that recognize vesicle membranes of specific curvature, such as exosomes, for biomarker identifications.[13,14] Therefore, from both perspectives of better understanding fundamental biological mechanisms and designing novel materials for biomedical applications, it is essential to determine the physical factors that dictate the binding affinity and specificity of biomolecules to lipid membranes of potentially complex shape and composition.

Although relevant quantities such as the dissociation constant and partition coefficients can be measured experimentally using liposomes of controlled size and composition, it is often technically tedious and expensive to construct many variants of the biomolecule, especially typical-size proteins, for a systematic probe of membrane binding motifs. Therefore, there is a pressing need to develop effective computational methods for determining the position, orientation, conformation, and affinity of proteins/peptides when bound to a membrane surface. We emphasize that the question of interest here concerns peripheral binding of proteins/peptides to the bilayer, rather than the insertion of transmembrane proteins/peptides, which poses additional challenges to both experimental and computational studies.[15]

Despite recent progress in computational hardware and force fields for proteins and lipids, most, if not all,[15−19] computational studies of protein−membrane interactions remain at a qualitative level, even for peripheral binding interactions that do not implicate a significant deformation of the bilayer. With atomistic simulations, other than the standard issue of force field accuracy, the main challenge lies in sampling.[20] Many cellular membranes are multicomponent and featured with highly charged lipids such as cardiolipin[3] or phosphatidylinositol 4,5-bisphosphate (PIP_2).[2] Strong electrostatic interactions

Special Issue: Free Energy Calculations: Three Decades of Adventure in Chemistry and Biophysics

Received: March 14, 2014
Published: May 20, 2014

   dx.doi.org/10.1021/ct500218p | J. Chem. Theory Comput. 2014, 10, 2845−2859

between protein motifs and charged lipids can easily trap the system in a local conformational minimum. Moreover, protein/peptide-membrane binding may implicate a significant conformational transition in the biomolecule[21] and/or local demixing of lipids;[22] both occur at time scales notably longer than the typical simulation length of 10−100 ns. Therefore, most membrane binding free energy computations using all atom models focused on small peptides and single-component (either zwitterionic or charged) membranes.[15−19] Motivated by these challenges, Tajkhorshid and co-workers developed the HMMM,[23] in which the lipid tails are replaced by an organic solvent. This allows a much faster local (de)mixing of lipid head groups upon protein binding; the effect can be further amplified by allowing an area-per-lipid substantially larger than the realistic value. The HMMM has been successfully applied to study the binding of several peripheral membrane proteins such as the cytochrome P450,[24] where reversible binding of the protein was observed in tens of nanoseconds simulations. On the other hand, due to the approximate nature of the membrane/water interface, it remains difficult to compute quantitative information regarding protein−membrane interactions using HMMM alone. It is possible to rebuild full atomistic models for the protein−membrane system based on converged HMMM simulations, although no quantitative binding calculations have been reported so far, presumably due to the high computational cost of such calculations (see discussions in Computational Methods).

At the next level of approximation, the past decade has witnessed explosive developments of coarse-grained (CG) models for lipids and proteins.[25−32] Although these models are particularly effective for sampling large-scale processes such as membrane remodeling and membrane-mediated protein assembly, the quantitative accuracy of these models for predicting protein/membrane binding remains to be carefully investigated; moreover, most CG models require that the protein is either fully flexible or structurally rigid.[33] Finally, we have the implicit membrane modeling framework[34,35] in which the protein is treated atomistically while the membrane/water interface is treated implicitly using dielectric continuum models, such as various variants of the generalized Born model,[36] or a lattice model.[37,38] Several such models have been successfully applied to study the folding of small membrane proteins/peptides.[39] A particular variant called the IMM1 model[34] has been applied to compare the binding of antimicrobial peptides to implicit membranes of different shapes (e.g., membrane pore[40,41]) and compositions.[34,42] In all those studies, to the best of our knowledge, the binding of the proteins/peptides to the membrane was characterized at a qualitative level, and few rigorous binding free energy calculations were reported. The exceptions are the study of Murray et al.[43] and Ben-Tal et al.,[44−47] who used models for the peptide conformational ensembles and a continuum or lattice model for the membrane to analyze the binding of various peptides or small proteins and compared the results to available experimental data. In another study,[48] Lazaridis et al. compared results of the IMM1 model with experimental data regarding the pH dependence of peptide binding to a charged membrane; the binding free energy was estimated by taking the difference of IMM1 solvation free energies at the membrane surface and solution.

Therefore, based on the above survey, it is evident that an important void to fill is the development and evaluation of a computational framework for the computation of membrane binding free energy that is applicable to both peptides and large proteins. This is precisely what we set out to do in this and subsequent work. Specifically in this study, we first discuss general computational approaches for binding free energy calculations of biomolecules at the membrane surface, following previous developments for protein[49−51]/surface[52]-ligand binding free energy calculations. Then, we introduce a particularly efficient adaptation of an implicit membrane model to one of those strategies based on a combination of free energy perturbation and the Bennett acceptance ratio (BAR)[53,54] protocol. Particular care is paid to the treatment of anionic membranes with the implicit membrane model (referred to as GBSW-GCS, see below) because most biological membranes contain a high percentage of anionic lipids.[2,8] The effectiveness of this method is quantitatively evaluated by studying several peptide systems and comparing the results to available experimental data and more expensive potential of mean force computations. The advantage and limitations of the method are discussed by also comparing the results to previous computational efforts. In a separate work, we will report application of the method to a realistic protein (RecA) and comparison to HMMM simulations and experimental studies. We hope these studies help promote more quantitative analysis of protein/membrane binding interactions and stimulate further developments along this line.

COMPUTATIONAL METHODS

In this section, we first review the basic approaches for computing binding free energies of a biomolecule to the membrane, following previous discussions for protein−ligand binding calculations.[49−51] Next, we discuss how to best apply those approaches, especially the one based on free energy perturbation, with an implicit membrane model. In this context, we also discuss some technical details regarding the implicit membrane model for anionic membranes.

Binding Free Energy Calculation. As discussed in previous work on protein[49−51]/surface[52]-ligand binding calculations, there are two general approaches for computing binding free energies: umbrella sampling (US) along a (un)binding coordinate and free energy perturbation (FEP) following a double-decoupling thermodynamic cycle (Figure 1).

Potential of Mean Force (PMF) from Umbrella Sampling. In the PMF approach, the biomolecule is pulled from the membrane bound state toward the solution, and the reverse

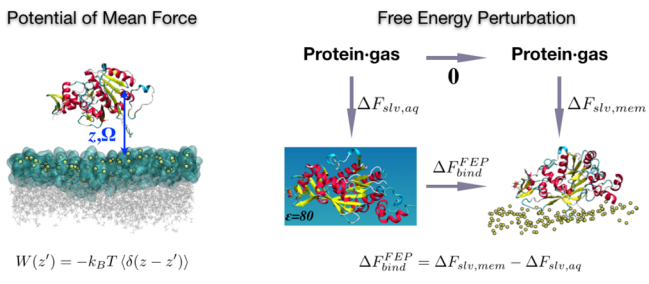

Figure 1. Two general approaches for the calculation of binding free energy of a biomolecule to the membrane surface: (un)binding potential of mean force (PMF) simulations using umbrella sampling and free energy perturbation (FEP) that involves decoupling the biomolecule from different environments (solution and membrane surface). In realistic applications, to ensure convergence, additional steps that involve the application and removal of positional (z), orientational (Ω), and conformational restraints are needed.[49−52] Also see text for discussions.

work along this (un)binding coordinate, $W(z)$, is computed using umbrella sampling and weighted histogram analysis.[55] The binding free energy ($\Delta^{\mathrm{US}}_{\mathrm{bind}}$) and binding constant ($K_{\mathrm{bind}}$) are obtained by the integration of $W(z)$ along z

$$\begin{aligned}\exp[-\beta\Delta F^{\mathrm{US}}_{\mathrm{bind}}] &= K_{\mathrm{bind}} \\ &= \frac{[P]_{\mathrm{mem}}}{[P]_{\mathrm{aq}}} \\ &= \frac{\int_{\mathrm{mem}}\rho(z)\,\mathrm{d}z}{\int_{\mathrm{aq}}\rho(z)\,\mathrm{d}z} \\ &= \frac{(c^{\ominus})^{1/3}\int_{\mathrm{mem}}\rho(z)\,\mathrm{d}z}{\int\delta(z-z^*)\rho(z)\,\mathrm{d}z} \\ &= \frac{(c^{\ominus})^{1/3}\int_{\mathrm{mem}}\exp[-\beta W(z)]\,\mathrm{d}z}{\int\delta(z-z^*)\exp[-\beta W(z)]\,\mathrm{d}z}\end{aligned} \tag{1}$$

Here, β is the inverse temperature ($1/k_{\mathrm{B}}T$), $[P]$ is the concentration of the biomolecule in the aqueous solution (aq) or at the membrane surface (mem), and z^* is a randomly chosen point on the binding pathway when the biomolecule is far away from the membrane−water interface. The integration for the membrane bound region (the "mem" ensemble) is determined by the region with $W(z)$ being substantially lower than $k_{\mathrm{B}}T$ compared to the asymptote, although for strongly bound cases (most cases studied here) $\Delta F^{\mathrm{US}}_{\mathrm{bind}}$ is dictated by the well region of the PMF and not sensitive to the particular choice of the integration range.[16] Because of the delta function in the denominator, the standard state concentration $c^{\ominus}$ is introduced with a value of 1/1661 Å^{-3}, assuming the bulk concentration of the biomolecule as 1 M.

Although the formulation outlined in eq 1 is conceptually straightforward, additional care needs to be exercised for practical applications. First, when the biomolecule adopts rather different conformations in the bulk solution and at the membrane surface, it is likely that straightforward 1D-PMF simulations encounter sampling issues. In this case, it is useful to use a multistage protocol[51,56] in which the conformation of the biomolecule is subject to a restraint during the unbinding PMF calculations (e.g., a harmonic RMSD restraint relative to the dominant membrane bound conformation). Next, in the unbound simulation, the conformation of the biomolecule is relaxed relative to that favored in the bulk solution, and the corresponding reverse work is evaluated using a second PMF calculation. The sum of the two PMF results gives the net binding free energy. The second issue concerns the difference in the rotational entropy between the membrane-bound and unbound states; it is unlikely that this difference is fully sampled in typical (un)binding PMF computations. Again the practical approach is to apply orientational restraints and then estimate the corresponding contributions to the binding free energy separately.[51,56] Both of these issues are elaborated on below in the binding free energy calculations using the implicit membrane/solvent model (e.g., see Figure 2).

Free Energy Perturbation (FEP) Following a Binding Thermodynamic Cycle. In an alternative approach, FEP calculations are carried out to decouple the biomolecule from both bulk solution and the membrane surface. In other words, one computes the "solvation free energy" of the biomolecule twice, once in bulk solution ($\Delta F_{\mathrm{slv,aq}}$) and once at the membrane surface ($\Delta F_{\mathrm{slv,mem}}$). Following the thermodynamic cycle in Figure 1b, the difference between these solvation free energies is nothing but the binding free energy, i.e., $\Delta F^{\mathrm{FEP}}_{\mathrm{bind}} = \Delta F_{\mathrm{slv,mem}} - \Delta F_{\mathrm{slv,aq}}$.

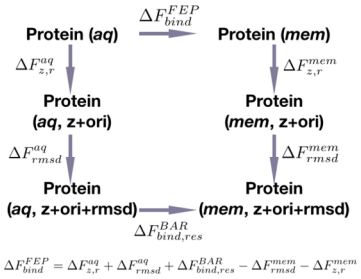

Figure 2. A thermodynamic cycle with z coordinate, orientational, and RMSD restraints, leading to the binding free energy ($\Delta F^{\mathrm{FEP}}_{\mathrm{bind}}$) of a protein from the aqueous phase (aq, unbound state) to the membrane−water interface (mem, bound state). The binding processes are shown as horizontal and application/removal of restraints as vertical processes.

To help make connections to the subsequent discussions using an implicit membrane/solvent model for the bound/unbound state, we explicitly define the solvation free energy for a specific environment X(= aq, mem) as,

$$\begin{aligned}\exp(-\beta\Delta F_{\mathrm{slv},X}) &= \frac{\int_X \exp[-\beta(U_{pp}+U_{px}+U_{xx})]\,\mathrm{d}\vec{R}\,\mathrm{d}\vec{X}}{\int \exp[-\beta(U_{pp}+U_{xx})]\,\mathrm{d}\vec{R}\,\mathrm{d}\vec{X}} \\ &= \frac{\int_X \exp[-\beta(U_{pp}+U_{px}+U_{xx})]\,\mathrm{d}\vec{R}\,\mathrm{d}\vec{X}}{\int \exp(-\beta U_{pp})\,\mathrm{d}\vec{R}\cdot\int \exp(-\beta U_{xx})\,\mathrm{d}\vec{X}} \\ &= \frac{\int_X \exp[-\beta(U_{pp}(\vec{R})+\Delta W_{\mathrm{slv},X}(\vec{R})]\,d\vec{R}}{\int \exp[-\beta U_{pp}]\,\mathrm{d}\vec{R}}\end{aligned} \tag{2}$$

where $\vec{X}$ indicates the microscopic coordinates of the environmental degrees of freedom; $\vec{R}$ indicates the coordinates of the biomolecule; and U's are the relevant potential functions for the biomolecule (U_{pp}), the environment (U_{xx}), and the interaction between them (U_{px}). The subscript X for the integrals indicates that care needs to be exercised to define the relevant conformational ensemble in environment X (see discussion above eq 1). Note that $\Delta F_{\mathrm{slv},X}$ is better thought of as a transfer free energy from a vacuum to a specific environment, and it includes contributions from changes in the internal energy and conformational entropy of the biomolecule. The quantity $\Delta W_{\mathrm{slv},X}(\vec{R})$ is the solvation potential of mean force defined as a function of the biomolecular conformation ($\vec{R}$) in environment X, i.e., the quantity approximated by an implicit solvent/membrane model[57]

$$\exp(-\beta\Delta W_{\mathrm{slv},X}(\vec{R})) = \frac{\int \exp[-\beta(U_{px}(\vec{R})+U_{xx})]\,\mathrm{d}\vec{X}}{\int \exp(-\beta U_{xx})\,\mathrm{d}\vec{X}} \tag{3}$$

Similar to the above discussion of the (un)binding-PMF protocol, practical applications are more complex than what Figure 1b implies. First of all, the conformation of a biomolecule in the uncoupled (gas) phase is likely very different from that either in solution or at the membrane surface. Therefore, practical simulations likely require restraining the conformation of the biomolecule during the two

solvation free energy calculations, and the effects of the restraints can be rigorously estimated for the solvated state with additional FEP calculations that gradually eliminate the restraints.[51,56] Second, due to the conformational restraints, the two solvation free energy simulations (for bulk and membrane surface, respectively), in general, lead to two distinct gas phase states. Therefore, an additional calculation needs to be carried out to obtain the free energy difference between these two gas-phase conformational states to rigorously complete the thermodynamic cycle in Figure 1b; this can be done in a number of ways, such as using the confinement approach proposed by Karplus and co-workers.[58] Finally, the translational and rotational contributions to $\Delta F_{\text{bind}}^{\text{FEP}}$ need to be carefully considered by applying appropriate restraints and subsequent (analytical) estimates (see below).

Binding Free Energy with an Implicit Membrane Model. The discussion above makes it clear that binding free energy calculations at the membrane surface are often far from straightforward, especially for a typical-size protein rather than a short peptide. The (un)binding-PMF approach may require many windows,[16−19] and the sampling with explicit solvent/membrane models is likely to meet significant challenges,[15] especially for a multicomponent membrane. Similarly, the FEP approach is also challenging for protein binding: while decoupling a small molecule ligand or peptide from a protein complex or solution is realistic, it is far less practical to decouple a protein from either the solution or membrane surface.

Motivated by these challenges, we have decided to explore binding free energy calculations using an implicit membrane/solvent model. There are several considerations that support this exploration. First, implicit membrane models are computationally efficient, since the slow processes of lipid diffusion and (de)mixing are not included. Although local demixing of lipids has been suggested as important in several cases, especially for proteins whose function requires very specific lipids like PIP_2,[2] Monte Carlo studies[43,59] found that the demixing of monovalent lipids such as PS is negligible in the presence of a highly charged peptide. Therefore, it is likely that a mean-field type of model can serve as a reasonable starting point for probing the effect of membrane charge on binding affinity and specificity, as well as for identifying membrane-binding protein motifs. In fact, by comparing results from an implicit membrane model with those using full atomistic representation of lipids, one is able to gain useful insights regarding the contribution from generic electrostatic effects vs those due to specific protein−lipid interactions. Therefore, developing an effective computational protocol using an implicit membrane/solvent model is not just about computational efficiency, it also leads to novel physical understandings of membrane−protein interactions.

In the following, we first briefly comment on an approximate way that implicit membrane/solvent models were used to estimate protein binding to membranes[34,40−42,60] and then present an alternative approach for the same purpose that we argue is more rigorous and effective. This is supported by applications to nontrivial peptide systems in the Results sections.

Estimating Binding Affinity by Solvation PMF Difference with Implicit Membrane/Solvent Simulations. In previous studies,[34,40−42,60] ΔF_{bind} was estimated using implicit membrane/solvent models by taking the difference in the solvation PMF (i.e., $\Delta W_{\text{slv,mem}}(\vec{R}) - \Delta W_{\text{slv,aq}}(\vec{R})$) at each snapshot and then averaging this quantity over the molecular dynamics trajectory for the membrane-bound state. Although this is an intuitive protocol, it is instructive to examine its physical meaning more closely.

We start by realizing that, in the simplest scenario that follows the binding thermodynamic cycle in Figure 1b, ΔF_{bind} is formally related to the ratio of two configuration integrals that involve the solvation PMFs for the two environments

$$\exp(-\beta\Delta F_{\text{bind}}^{\text{FEP}}) = \frac{\int_{\text{mem}} \exp[-\beta(U_{pp} + \Delta W_{\text{slv,mem}})]\, \mathrm{d}\vec{R}}{\int_{\text{aq}} \exp[-\beta(U_{pp} + \Delta W_{\text{slv,aq}})]\, \mathrm{d}\vec{R}} \tag{4}$$

This expression can be manipulated in different ways to obtain different protocols that differ in practical convergence. For example, one possible manipulation leads to

$$\begin{aligned}\exp(-\beta\Delta F_{\text{bind}}^{\text{FEP}}) &= \frac{\int_{\text{mem}} \exp[-\beta(U_{pp} + \Delta W_{\text{slv,mem}})]\, \mathrm{d}\vec{R}}{\int \exp(-\beta U_{pp})\, \mathrm{d}\vec{R}} \cdot \frac{\int \exp(-\beta U_{pp})\, \mathrm{d}\vec{R}}{\int_{\text{aq}} \exp[-\beta(U_{pp} + \Delta W_{\text{slv,aq}})]\, \mathrm{d}\vec{R}} \\ &= \frac{\langle \exp(\beta\Delta W_{\text{slv,aq}})\rangle_{\text{aq}}}{\langle \exp(\beta\Delta W_{\text{slv,mem}})\rangle_{\text{mem}}}\end{aligned} \tag{5}$$

where $\langle ... \rangle_X$ indicates the ensemble average in the relevant environment X. From eq 5, a cumulant expansion truncated at the second-order leads to

$$\Delta F_{\text{bind}}^{\text{FEP}} \approx \langle \Delta W_{\text{slv,mem}}\rangle_{\text{mem}} - \langle \Delta W_{\text{slv,aq}}\rangle_{\text{aq}} + \frac{1}{2}\beta{\delta_{\text{mem}}}^2 - \frac{1}{2}\beta{\delta_{\text{aq}}}^2 + ... \tag{6}$$

where the fluctuation of solvation PMF is defined as ${\delta_X}^2 \equiv \langle {\Delta W_{\text{slv},X}}^2\rangle_X - \langle \Delta W_{\text{slv},X}\rangle_X^2$. In practice, this avenue is unlikely to be productive because the magnitude of the solvation PMFs and their fluctuations is usually much larger than $k_{\text{B}}T$. In other words, it would be a poor approach to estimate binding by computing separate trajectories for solution and membrane bound states, collecting solvation PMFs for the snapshots and then taking the difference between the solution and membrane simulations.

An alternative formal manipulation of eq 5 is to treat the membrane-bound state as the only reference ensemble, leading to (in the limit of strong binding to the membrane interface)

$$\exp(\beta\Delta F_{\text{bind}}^{\text{FEP,mem}}) = \langle \exp[\beta\Delta\Delta W_{\text{slv}}(\vec{R})]\rangle_{\text{mem}} \tag{7}$$

where $\Delta\Delta W_{\text{slv}}(\vec{R}) = \Delta W_{\text{slv,mem}}(\vec{R}) - \Delta W_{\text{slv,aq}}(\vec{R})$ is the differential solvation PMF for a particular protein conformation $\vec{R}$. Again, one can perform a second-order cumulant expansion

$$\Delta F_{\text{bind}}^{\text{FEP,mem}} = \langle \Delta\Delta W_{\text{slv}}\rangle_{\text{mem}} + \frac{1}{2}\beta{\xi_{\text{mem}}}^2 ... \tag{8}$$

where fluctuation of the differential solvation PMF in a membrane-bound state simulation is defined as ${\xi_{\text{mem}}}^2 \equiv \langle {\Delta\Delta W_{\text{slv}}}^2\rangle_{\text{mem}} - \langle \Delta\Delta W_{\text{slv}}\rangle_{\text{mem}}^2$. Compared to eq 6, the calculations for eq 8 are expected to be much better behaved because we are accumulating much smaller values, $\Delta\Delta W_{\text{slv}}(\vec{R})$, rather than the absolute solvation PMFs ($\Delta W_{\text{slv},X}(\vec{R})$) themselves.

These derivations make it clear that the protocol used to estimate binding free energy of proteins/peptides in previous

work is a first-order expression for a FEP based protocol that follows the binding thermodynamic cycle in Figure 1b. Whether the cumulant expansion reaches satisfactory convergence with only the first-order contributions needs to be evaluated with realistic examples. In fact, according to the well-known Gibbs–Bogoliubov–Feynman bound,[61] the first-order result gives rigorously a lower bound to the binding free energy

$$\Delta F_{\text{bind}}^{\text{FEP,mem}} = \beta^{-1} \ln\langle \exp[\beta \Delta\Delta W_{\text{slv}}(\vec{R})]\rangle_{\text{mem}} \geq \langle \Delta\Delta W_{\text{slv}}(\vec{R})\rangle_{\text{mem}} \quad (9)$$

Moreover, as discussed above, naively following the thermodynamic cycle in Figure 1b potentially glosses over contributions from different protein conformations and different translational/rotational entropies in solution and membrane-bound states. Therefore, we introduce an alternative approach in the following subsection.

A Binding Free Energy Protocol Based on Implicit Membrane/Solvent Simulations in Solution and at the Membrane Surface. To improve upon the protocol discussed above, the first point to realize is that eq 7 relies only on the membrane-bound state simulation. An immediate improvement is to take the solution state ensemble into consideration as well. This can be done by starting with an alternative manipulation of eq 4 (in the limit of strong binding to the membrane interface)

$$\exp -(\beta \Delta F_{\text{bind}}^{\text{FEP,aq}}) = \langle \exp[-\beta \Delta\Delta W_{\text{slv}}(\vec{R})]\rangle_{\text{aq}} \quad (10)$$

Therefore, eqs 7 and 10 offer two estimates for the same quantity $\Delta F_{\text{bind}}^{\text{FEP}}$ based on differential solvation PMFs collected from two conformational ensembles. When the solution and membrane-bound ensembles are sufficiently different (but have finite overlap, otherwise intermediate states can be introduced as in regular FEP simulations[62]), it should be possible to improve the estimate of $\Delta F_{\text{bind}}^{\text{FEP}}$ based on both ensembles. One possible protocol is the Double-Wide Free Energy Perturbation (DW-FEP),[63] which provides the mixing coefficients for data collected with these two ensembles

$$\Delta F_{\text{bind}}^{\text{FEP,dw}} = a\Delta F_{\text{bind}}^{\text{FEP,aq}} + (1-a)\Delta F_{\text{bind}}^{\text{FEP,mem}} \quad (11)$$

Here, a is the coefficient to minimize the bias of $\Delta F_{\text{bind}}^{\text{FEP,dw}}$, given by

$$a = \frac{N_{\text{aq}}\sigma_{\text{mem}}^2}{N_{\text{aq}}\sigma_{\text{mem}}^2 + N_{\text{mem}}\sigma_{\text{aq}}^2} \quad (12)$$

where N_X is the number of samples in the simulation for environment X and σ_X is the variance of $\Delta F_{\text{bind}}^{\text{FEP}}$ estimated with the corresponding conformational ensemble.

For even more robust results, we use the BAR approach[53,54,64] to obtain the best estimate of $\Delta F_{\text{bind}}^{\text{FEP}}$ based on the $\Delta\Delta W_{\text{slv}}$ data from the two conformational ensembles. To briefly review the BAR protocol, one starts with an initial guess of $\Delta F_{\text{bind}}^{\text{FEP}}$ denoted as C:

$$C = \frac{1}{\beta}\ln\frac{Z_{\text{aq}}N_{\text{mem}}}{Z_{\text{mem}}N_{\text{aq}}} \quad (13)$$

where $Z_X = \Sigma \exp(-\beta \Delta W_{\text{slv},X})$, while in practice, results from the DW-FEP expression (eq 11) can be used as the initial guess for C. Then eq 14 is used to update $\Delta F_{\text{bind}}^{\text{BAR}} \approx C$ until convergence is reached (i.e., the estimated $\Delta F_{\text{bind}}^{\text{BAR}}$ no longer changes or eq 15 is satisfied)[64]

$$\Delta F_{\text{bind}}^{\text{BAR}} = \frac{1}{\beta}\left[\ln\frac{\langle f(-\Delta\Delta W_{\text{slv}} + C)\rangle_{\text{mem}}}{\langle f(\Delta\Delta W_{\text{slv}} - C)\rangle_{\text{aq}}}\right] + C \quad (14)$$

$$\langle f(-\Delta\Delta W_{\text{slv}} + C)\rangle_{\text{mem}} = \langle f(\Delta\Delta W_{\text{slv}} - C)\rangle_{\text{aq}} \quad (15)$$

Here, $f(x)$ is the Fermi function: $f(x) = 1/[1 + \exp(\beta x)]$. The statistical error associated with BAR is estimated with the equation below:[53,54]

$$\sigma_{\Delta F}^2 = \frac{1}{N_{\text{aq}}\beta^2}\left[\frac{\langle f^2(x)\rangle_{\text{aq}}}{\langle f(x)\rangle_{\text{aq}}^2} - 1\right] + \frac{1}{N_{\text{mem}}\beta^2}\left[\frac{\langle f^2(x)\rangle_{\text{mem}}}{\langle f(x)\rangle_{\text{mem}}^2} - 1\right] \quad (16)$$

where x is $\Delta\Delta W_{\text{slv}} - C$ for the solution (aq) ensemble and $C - \Delta\Delta W_{\text{slv}}$ for the membrane surface ensemble. In the applications discussed below, the BAR iteration typically converges quickly (e.g., 20 iterations with change in $\Delta F_{\text{bind}}^{\text{BAR}}$ below 10^{-4} kcal/mol), especially when there is significant overlap between the two conformational ensembles.

As emphasized in the discussion above, to better control contributions due to differences in the conformations and translation/rotational entropies between the solution and membrane-bound states, we follow a multistage protocol as illustrated in Figure 2, similar to that developed by Deng et al. for protein–ligand binding calculations.[49−51] Accordingly, the final binding free energy is computed by the following equation:

$$\Delta F_{\text{bind}}^{\text{FEP}} = \Delta F_{z,r}^{\text{aq}} + \Delta F_{\text{rmsd}}^{\text{aq}} + \Delta F_{\text{bind,res}}^{\text{BAR}} - \Delta F_{\text{rmsd}}^{\text{mem}} - \Delta F_{z,r}^{\text{mem}} \quad (17)$$

Here, the subscripts z,r indicate that restraints (u_z,u_r) on the protein's center-of-mass z coordinate and overall orientation are applied; rmsd indicates that the conformation of the protein is controlled via RMSD restraints (u_{rmsd}) with respect to the dominant conformation at the membrane-bound state. The corresponding free energy components are defined in the following, where the subscript of the ensemble average indicates both the environment (aq/mem) and the potential functions used to generate the ensemble

$$\exp(-\beta\Delta F_{\text{rmsd}}^{\text{aq}}) = \frac{\int_{\text{aq}} \exp(-\beta[U_{pp} + \Delta W_{\text{slv,aq}} + u_z + u_r + u_{\text{rmsd}}])\, d\vec{R}}{\int_{\text{aq}} \exp(-\beta[U_{pp} + \Delta W_{\text{slv,aq}} + u_z + u_r])\, d\vec{R}} = \langle \exp(-\beta u_{\text{rmsd}})\rangle_{(\text{aq};U_{pp}+\Delta W_{\text{slv,aq}}+u_z+u_r)} \quad (18)$$

$$\exp(-\beta\Delta F_{\text{bind,res}}^{\text{BAR}}) = \frac{\int_{\text{mem}} \exp(-\beta[U_{pp} + \Delta W_{\text{slv,mem}} + u_z + u_r + u_{\text{rmsd}}])\, d\vec{R}}{\int_{\text{aq}} \exp(-\beta[U_{pp} + \Delta W_{\text{slv,aq}} + u_z + u_r + u_{\text{rmsd}}])\, d\vec{R}} = \langle \exp(-\beta[\Delta\Delta W_{\text{slv}}])\rangle_{(\text{aq};U_{pp}+\Delta W_{\text{slv,aq}}+u_z+u_r+u_{\text{rmsd}})} = \frac{1}{\langle \exp(\beta[\Delta\Delta W_{\text{slv}}])\rangle_{(\text{mem};U_{pp}+\Delta W_{\text{slv,mem}}+u_z+u_r+u_{\text{rmsd}})}} \quad (19)$$

$$\exp(-\beta\Delta F^{\mathrm{mem}}_{\mathrm{rmsd}}) = \frac{\int_{\mathrm{mem}} \exp(-\beta[U_{pp} + \Delta W_{\mathrm{slv,mem}} + u_z + u_r + u_{\mathrm{rmsd}}])\, \mathrm{d}\vec{R}}{\int_{\mathrm{mem}} \exp(-\beta[U_{pp} + \Delta W_{\mathrm{slv,mem}} + u_z + u_r])\, \mathrm{d}\vec{R}} = \langle \exp(-\beta u_{\mathrm{rmsd}}) \rangle_{(\mathrm{mem};U_{pp}+\Delta W_{\mathrm{slv,mem}}+u_z+u_r)} \quad (20)$$

$$\exp(-\beta\Delta F^{\mathrm{mem}}_{z,r}) = \frac{\int_{\mathrm{mem}} \exp(-\beta[U_{pp} + \Delta W_{\mathrm{slv,mem}} + u_z + u_r])\, \mathrm{d}\vec{R}}{\int_{\mathrm{mem}} \exp(-\beta[U_{pp} + \Delta W_{\mathrm{slv,mem}}])\, \mathrm{d}\vec{R}} = \langle \exp(-\beta u_{z,r}) \rangle_{(\mathrm{mem};U_{pp}+\Delta W_{\mathrm{slv,mem}})} \quad (21)$$

For these free energy quantities, although we have only explicitly discussed the use of BAR to estimate $\Delta F^{\mathrm{BAR}}_{\mathrm{bind,res}}$, the other free energy components are also computed with the BAR protocol and relevant simulations (e.g., with and without the RMSD restraints for $\Delta F^{\mathrm{mem}}_{z,r}$). When the effects of the restraints are large, multistage simulations can be used as in protein−ligand simulations.[49−51]

Due to the homogeneous nature of the solution environment, the first term in eq 17 can be estimated analytically:[49−52]

$$\Delta F^{a}_{z,r} = \Delta F^{a}_{z} + \Delta F^{a}_{r} \quad (22)$$

If we assume a harmonic restraint for z, $u_z = (1/2)k_z(z - z_0)^2$, on the protein, the following expression is obtained:

$$\exp(-\beta\Delta F^{a}_{z}) = \frac{\int_{\mathrm{aq}} \exp(-\beta[U_{pp} + \Delta W_{\mathrm{aq}} + u_z])\, \mathrm{d}\vec{R}}{\int_{\mathrm{aq}} \exp(-\beta[U_{pp} + \Delta W_{\mathrm{aq}}])\, \mathrm{d}\vec{R}} \approx \frac{1}{\Delta z}\cdot\sqrt{\frac{2\pi}{\beta k_z}} \quad (23)$$

where Δz is the cubic root of volume that the protein can access in aqueous solution, which is taken to be 1661 Å^3 at the standard state concentration $c^{\ominus} = 1M$. For the orientational restraint, the form varies and we use the following to estimate ΔF^{a}_{r}:[49−51,65,66]

$$\exp(-\beta\Delta F^{a}_{r}) = \frac{\int_{\mathrm{aq}} \exp(-\beta[U_{pp} + \Delta W_{\mathrm{aq}} + u_z + u_r])\, \mathrm{d}\vec{R}}{\int_{\mathrm{aq}} \exp(-\beta[U_{pp} + \Delta W_{\mathrm{aq}} + u_z])\, \mathrm{d}\vec{R}} = \frac{\int_{\mathrm{aq}} \exp(-\beta u_r)\, \mathrm{d}\Omega}{\int_{\mathrm{aq}} \mathrm{d}\Omega}, \approx \frac{(\sqrt{2\pi})^3 \sigma_\varphi \sigma_{\sin\theta} \sigma_\psi}{8\pi^2} \quad (24)$$

where Ω represents the three orientational degrees of freedom ϕ, θ, and ψ for a free protein in aqueous solution. The derivation assumes a normal distribution of all three angles, with σ representing fluctuation. $8\pi^2$ is the integration of three nonhindered angles with two in the spherical coordinate system (contributing to 4π) and one additional angle due to the nonlinear shape of the protein (contributing to 2π).[65] The fluctuations of the angles are estimated from the simulations.

Following the thermodynamic cycle in Figure 2 (thus eq 17) would be the most rigorous way to compute the binding free energy. In practical applications, further approximations might be acceptable. For example, when the conformation of the protein/peptide does not differ much between the unbound and bound states, one may omit the RMSD restraints.

Technical Considerations for an Implicit Membrane Model for Anionic Membranes: GBSW-GCS. There are several popular implicit membrane/solvent models developed for modeling biomolecules.[34,67,35] In this work, we choose the generalized Born with a simple switching function (GBSW) model because it has been carefully parametrized for both solution and membrane environments and successfully applied to a broad set of problems.[68−71] Since many biological membranes are enriched with anionic lipids, we discuss several technical issues related to applying GBSW to anionic membranes.

Electrostatic Description of Anionic Membrane: Gouy−Chapman Theory. In previous work, both IMM1[34] and GBSW have been integrated with the Gouy−Chapman (GC) theory[72] to treat membranes with anionic lipids, such as PS, PG, and cardiolipin. Figure 3 illustrates the integration of GBSW and

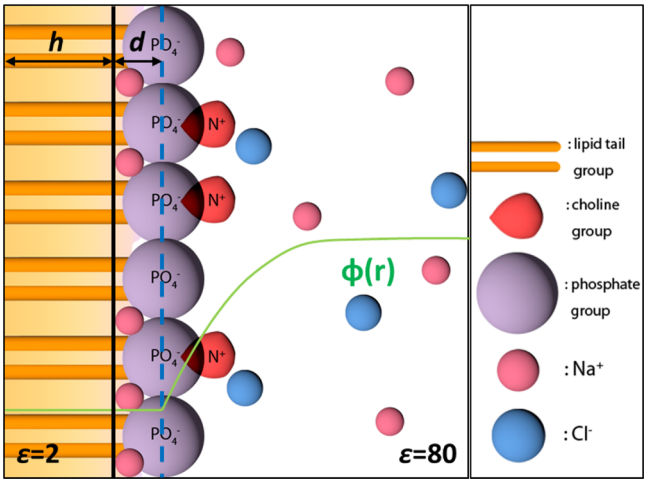

Figure 3. A schematic representation that illustrates the key parameters in the GBSW-GCS model. The thick black line indicates the dielectric boundary that separates the high dielectric (ε = 80) and low dielectric (ε = 2) regions in the GBSW model. The dashed blue line indicates the dividing surface in the GCS model where surface charges (with a density of σ) are homogeneously distributed for an anionic membrane. The variable h is the half thickness of the low dielectric region that represents the lipid tails, and the variable d is the distance between the dividing surface and dielectric boundary. The green line is a schematic description of the electrostatic potential $\phi(r)$ in the GCS model. In the current work, we discuss the choice of σ and d.

the GC theory. The GC theory provides an analytical expression for the electrostatic potential beyond the dividing surface that bears the membrane charge

$$\varphi(r) = \frac{2}{\beta\mathcal{Z}e}\ln\frac{[1 + \alpha\exp(-\kappa r)]}{[1 - \alpha\exp(-\kappa r)]} \quad (25)$$

$$\kappa = \sqrt{\frac{2\rho\beta z^2 e^2}{\varepsilon}} \quad (26)$$

where $\phi(r)$ is the electrostatic potential in the aqueous solution at a distance r from the charged dividing surface, e is the elementary charge, ε is the absolute permittivity of water, ρ is the number concentration of the salt, κ is the inverse Debye length defined with eq 26, and $\alpha = \tanh[\beta z e\phi(0)/4]$. Note that

this equation only holds when the solution contains salt with formula AB where A^{z+} is the cation and B^{z-} is the anion, with z the absolute value of elementary charge of a single ion. The surface potential $\phi(0)$ in the definition of α is given by Grahame's equation:[73]

$$\varphi(0) = \frac{2}{\beta z e}\cdot \text{arcsinh}\frac{\sigma}{\sqrt{8\varepsilon\rho/\beta}} \tag{27}$$

where σ is the surface charge density on the dividing surface. The electrostatic potential $\phi(r)$ contributes to the total GBSW solvation free energy through the solute (protein) charge distribution, $\Sigma_i q_i \phi(\mathbf{r}_j)$. We note that for contributions that arise from charges below the dividing surface (i.e., toward the interior of the bilayer), the potential is taken to be identical to the surface potential (as illustrated in Figure 3). In other words, the interfacial dipole potential[74] is ignored in the GC model, although it can be included in an empirical fashion.[75]

In the GC theory, there are two key parameters: the location of the dividing surface, which is characterized by $h + d$ as the distance from the membrane center ($z = 0$), and the surface charge density, σ. In previous studies,[34] h is usually chosen according to the length of the lipid tail groups and d is taken be ~3 Å, which roughly maps to the size of a phosphate group. A previous study in our group[76] analyzed the ion distribution from atomistic simulations in the framework of the GC theory and suggested that it might be more appropriate to choose d = 10 Å. In this work, we compare how these two choices of the dividing surface impacts the computed binding free energy.

Regarding the surface charge density, σ, previous work[34,41] determined the value based on the mole fraction of anionic lipids and the typical area-per-lipid. This ignores the effect of counterion adsorption and thus may significantly overestimate the surface charge density. In this work, as discussed below, we use Stern's equation[77] to provide a better estimate for σ.

Stern's Equation. To better predict the surface potential using Grahame's equation, Stern incorporated the simple idea of a Langmuir isotherm to the charged surface,[77] leading to the Stern layer (schematically shown in Figure 3 around the dividing surface). Without distinguishing between surface potential and ζ potential,[72] which is an approximation, one can fit eqs 28 and 29 to the experimental data, and a good agreement is observed[78,79]

$$\varphi(0) = \frac{2}{\beta \mathcal{Z} e}\cdot \text{arcsinh}\frac{\sigma(1-x)}{\sqrt{8\varepsilon\rho/\beta}} \tag{28}$$

$$\frac{1}{K_a c}\cdot\frac{x}{1-x} + \frac{2\sigma}{\sqrt{8\varepsilon\rho/\beta}}\cdot\sqrt{\frac{x(1-x)}{K_a c}} - 1 = 0 \tag{29}$$

where x is the proportion of counterions that are absorbed on the charged surface, K_a is the association constant of the counterions on the membrane surface, and c is the molar concentration of the salt: $c = \rho/1000N_A$. For adsorption of Na^+ on a PC−PS mixture, we use 1 M^{-1} as the association constant.[79] For adsorption of K^+ on a PC−PG mixture, we use 0.3 M^{-1} as the association constant.[80]

As shown in Figure 4, for the 50% anionic lipid fraction, Stern's equation reduces the effective surface charge density by about a factor of 2. Therefore, including the Stern model will have a major impact on the estimated binding affinity to membranes with anionic lipids. The precise value of K_a varies in the literature: between 0.15 and 0.3 M^{-1} for K^+ and between

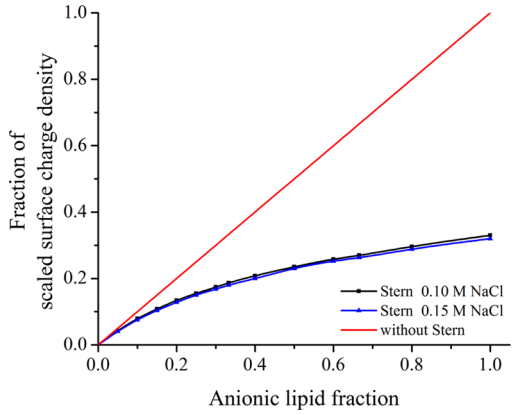

Figure 4. Fraction of scaled surface charge density ($1 - x$ in eq 28) as a function of experimentally prepared anionic lipid fraction based on Stern's equation. Different NaCl solution concentrations are compared.

0.6 and 1.0 M^{-1} for Na^+. The effect of such variations on the calculated $\phi(0)$ and thus binding free energy is rather modest; for example, for a membrane with 50% anionic lipids and 0.1 M KCl, changing K_a for K^+ from 0.15 M^{-1} to 0.3 M^{-1} would change $\phi(0)$ by ~7 mV, which translates to <0.2 kcal/mol in binding free energy per positive charge. In the following, we refer to the implicit membrane model that includes the Stern model as the GBSW-GCS model, to distinguish it from the simpler GBSW-GC model that does not consider counterion adsorption. As shown in the Results and Discussion section, the GBSW-GCS is consistently more reliable than GBSW-GC when compared to available experimental data.

Partition Coefficients. Different from the unitless binding constant K_{bind} (eq 1) calculated from our simulations, experimentally determined partition coefficients are usually reported as $K_a = [P]_{mem}/[L][P]_{aq}$, where $[L]$ is the concentration of the total lipid. To facilitate a comparison between our simulation with experimental data, we follow the simple correction provided by Tzlil et al.[43] to estimate $[L]$:

$$[L] = (N_A a_L \lambda)^{-1} \tag{30}$$

where N_A is Avogadro's number, a_L is the average area per lipid of the membrane (70 $Å^2$), and λ is the membrane bilayer thickness (including the surrounding water, typically 86.6 Å). This leads to

$$\exp[-\beta\Delta F_{bind}^{exp}] = K_a\ (M^{-1})/3.65\ (M^{-1}) \tag{31}$$

where ΔF_{bind}^{exp} can be compared to the computed binding free energy (e.g., ΔF_{bind}^{FEP} in eq 17). Due to the exponential relationship between ΔF_{bind}^{exp} and $[L]$ in eq 31, small variations in lipid parameters such as λ and a_L do not notably affect ΔF_{bind}^{exp}.

RESULTS AND DISCUSSION

In the following, we first discuss results for a simple peptide, Lys_5, which has been studied experimentally; the results are used to illustrate the importance of including the Stern layer for binding to anionic membranes and to compare the two choices for the location of the dividing surface in the GBSW-GC(S) model. Next, we discuss the results for a set of larger but structurally rigid helices, which feature both charged and hydrophobic binding residues. Finally, we challenge our protocol by studying the binding of a set of fairly long and

Table 1. Comparison of Computed Binding Free Energy (kcal/mol) Using GBSW-GCS and Experimental Data for Lys_5[a]

		GBSW-GCS-3[b]			GBSW-GCS-10[b]		
PS%	expt[80]	US[c]	BAR[d]	$\langle\Delta\Delta W_{slv}\rangle_{mem}$[e]	US[c]	BAR[d]	$\langle\Delta\Delta W_{slv}\rangle_{mem}$[e]
10	−1.6	−2.5	−2.4 ± 0.2(−0.2 ± 0.1)	−0.5 ± 1.2	−3.1	−3.1 ± 0.2(−2.4 ± 0.1)	−2.9 ± 1.2
33	−4.3	−5.0	−5.1 ± 0.1(−4.3 ± 0.5)	−5.4 ± 2.3	−7.3	−6.6 ± 0.2(−6.8 ± 0.2)	−7.6 ± 1.6
50	−5.3	−6.2 [−8.1]	−5.5 ± 0.3(−6.4 ± 0.2)	−7.7 ± 2.0	−8.7[-11.4]	−7.9 ± 0.1(−8.2 ± 0.2)	−9.1 ± 1.6

[a]The experimental PS fraction is given as PS%. All simulations are done in 0.1 M KCl solution, as in the experimental study. [b]GBSW-GCS-3/10 takes d = 3/10 Å for the location of the charged dividing surface; see Figure 3 for an illustration. [c]Binding affinity based on the (un)binding-PMF calculations (i.e., eq 1) using umbrella sampling. Values in brackets are calculated without considering the Stern layer; i.e., they are calculated with the GBSW-GC model. All umbrella sampling results have a statistical uncertainty of no more than 0.02 kcal/mol as estimated using a bootstrapping protocol.[85] [d]Values without parentheses are obtained with the protocol introduced in this work (see Figure 2); values with parentheses are computed using the protocol without the RMSD restraining steps. [e]Estimated binding affinity by average differential solvation PMF ($\Delta\Delta W_{slv}$) based on membrane-bound simulation (i.e., first-order term in eq 8). The differences in translational/rotational entropy between solution and membrane-bound states are included following ref 45; this applies also to the $\Delta\Delta W_{slv}$ results shown in Tables 2 and 4.

flexible peptides (MARCKS-ED and its variants) and comparing to available experimental data.

Studies of Lys_5. In previous studies,[79−84] McLaughlin et al. and Cafiso et al. analyzed the applicability of the Gouy−Chapman−Stern model to anionic membrane systems. For example, with a Poisson−Boltzmann type of model, they were able to reproduce the binding free energy of Lys_n.[80] Here we revisit the Lys_5 model to calibrate the GBSW-GC(S) based binding free energy protocols. Due to the relatively small size of Lys_5, we are able to compute binding with the (un)binding-PMF approach using umbrella sampling; for comparison, we also compute binding with the BAR based approach (eq 17) and the differential solvation PMF protocol (i.e., linear term in eq 8). For the US simulations, we placed each window 0.5 Å apart from −6 Å (measured from the dielectric interface) to 34 and 54 Å for GBSW-GCS-3 and GBSW-GCS-10, respectively. The simulation time is 10 ns for each window. For the BAR and $\langle\Delta\Delta W_{slv}\rangle_{men}$ calculations shown in Table 1, each simulation is 20 ns long; a comparison to results obtained with 10 ns and block average analysis of statistical errors indicates that the results are adequately converged.

First of all, we compare the umbrella sampling based (un)binding-PMF results with available experiments for the three PS concentrations. We see from Table 1 that the GBSW-GCS model leads to rather good agreement with the experimental data with the choice of d = 3 Å; using d = 10 Å leads to systematically too strong binding affinities by 1−3 kcal/mol. We note that this observation does not necessarily suggest that the choice of d = 10 Å is less physical, as previous work[76] found that this choice in fact leads to more consistent bulk ion concentrations between atomistic simulation and the GC theory. Since the bound Lys_5 is located at 6.2 ± 2.1 Å and 8.1 ± 2.8 Å from the dielectric interface for GBSW-GCS-3 and GBSW-GCS-10, respectively, it is essentially below the dividing surface with the choice of d = 10 Å and therefore senses only the surface potential (since dipole potential is not included in the current framework). Thus, the fact that we find empirically that d = 3 Å is a better choice for binding affinity might be the result of cancellation of errors associated with the various approximations of GBSW-GCS.

The second observation is that the Stern layer makes a significant contribution to binding at a high fraction of anionic lipids. With a 50% negatively charged membrane, the GBSW-GCS results are substantially closer to the experimental data, especially with the choice of d = 3 Å; for example, with the GBSW-GC-10 model, the binding affinity is overestimated by more than a factor of 2. This is not surprising given the effect of the Stern layer on the magnitude of the apparent surface charge (Figure 4). On the basis of these observations, in the following discussion, we focus on the GBSW-GCS-3 results.

Compared to the PMF data, the BAR results are generally very similar. Due to the fairly small size of the system, the effect of imposing proper structural restraints and then removing them in separate steps (see Figure 2) is relatively small (∼1 kcal/mol); the exception is observed at a low anionic lipid fraction, in which case the binding is weak, and thus it is important to properly treat the conformational flexibility of the peptide by following the protocol in Figure 2. The differential solvation PMF protocol used in previous work[34,40,41,60] ($\langle\Delta\Delta W_{slv}\rangle_{men}$ column in Table 1) gives somewhat similar results to both BAR and the (un)binding PMF, although with notably larger statistical uncertainties (also see Figure S3 in the Supporting Information).

Structurally Rigid α Helices. Next, we study three related helices; the backbone of these peptides is structurally restrained to adopt the α helix conformation. We note that according to experiments,[86] $(LARL)_3$ is mostly helical in the presence of liposomes but largely unstructured in aqueous solution. We impose the structural rigidity here for both membrane-bound and solution states to make these peptides better-suited for comparing different binding computational protocols without complications due to incomplete conformational sampling; the analysis complements that for Lys_5 since both hydrophobic and charged interactions are involved (see Supporting Information for a brief discussion of GBSW-GCS calculations for the insertion PMF of amino acid side chains). We note that the computational protocol outlined in Figure 2 is particularly applicable to systems where the membrane bound and solution structures are very different; in these cases, the contribution from the conformational equilibrium in solution (e.g., from a disordered state to an α helix) is included in ΔF^{aq}_{rmsd}. Whether the folding equilibrium in solution is quantitatively described by GBSW is likely system-dependent and therefore beyond the scope of this work, which focuses on the applicability of GBSW-GCS to peptide−membrane interactions. In separate work, however, it is worthwhile to examine the entire binding process that starts with a disordered peptide in solution.

In the absence of directly comparable experimental binding data, the (un)binding PMF results with umbrella sampling are taken as the reference. As shown in Table 2, the general trend in the binding affinity is consistent with physical intuition: $(LASL)_3$ binds weaker than $(LARL)_3$ due to the elimination of a charge at the anionic membrane surface, while $(AARL)_3$ binds even weaker because the elimination of a favorable hydrophobic

Table 2. Computed Binding Affinity (kcal/mol) of Three Structurally Rigid Helices to an Anionic Membrane with Different Approaches[a]

sequence	US	BAR	$\langle \Delta\Delta W_{slv} \rangle_{mem}$	z position (Å)[b]
$(LARL)_3$	−18.9	−19.7 ± 0.1	−20.4 ± 1.7	15.9 (1.0)
$(LASL)_3$	−13.9	−14.3 ± 0.1	−15.2 ± 2.2	16.9 (0.7)
$(AARL)_3$	−8.8	−7.8 ± 0.1	−7.1 ± 2.6	19.8 (0.8)

[a]All simulations are done with a 33% PS/PC membrane and 0.1 M KCl solution. Other notations follow those in Table 1, including the statistical error analysis. All calculations are carried out with the GBSW-GCS-3 model. [b]The z position of the center-of-mass of the peptide backbone. For reference, the dielectric boundary (see Figure 3) is at z = 16 Å; thus z < 16 Å indicates insertion of the peptide into the hydrophobic region of the bilayer.

insertion into the low-dielectric region of the bilayer. The insertion depths (z position of center-of-mass) of the three peptides are summarized in Table 2.

The BAR approach gives very consistent results (within 1 kcal/mol) compared to the more expensive binding-PMF simulations. This is satisfying to see because while the binding-PMF simulation requires many windows due to the long-range nature of the anionic membrane−peptide interactions (80 windows used here), the BAR approach practically requires only two simulations. Due to the structural rigidity of the helices, it is not necessary to carry out additional steps for the RMSD restraints. The estimates based on $\langle \Delta\Delta W_{slv} \rangle_{men}$ are also in good agreement with BAR and PMF results, but only when translational/rotational entropy differences (∼4−5 kcal/mol) between solution and membrane bound states are properly included; the statistical uncertainties are also substantially larger.

Challenges Posed by Highly Flexible Systems: MARCKS-ED Peptides. A nontrivial benchmark system for membrane binding calculations is the MARCKS-ED peptide (sequence shown as WT in Table 3), which is a largely unstructured peptide with a high affinity to anionic membranes (with either PS or PIP_2)[87−90] due to the presence of 13 cationic (Lys/Arg) residues and five hydrophobic (Phe) groups. MARCKS proteins are involved in a number of signal transduction processes that regulate cell motility, secretion, membrane associated transport, as well as the regulation of the cell cycle. The effector domain (MARCKS-ED) is the prominent structural feature that contains 25 residues and regulates binding with F-actin, Ca^{2+}-calmodulin, and acidic phospholipids.[91,92] It has been studied extensively by McLaughlin et al.,[93] who analyzed the relative importance of electrostatic and hydrophobic contributions to binding by comparing the affinity of a series of variants in which either charged or hydrophobic residues were systematically removed.

Table 3. Sequence of the MARCKS-ED Peptide and It Mutants Studied Here[a]

MARCKS-ED	sequence
WT	*KKKKKR***F**S**F***KKS**F**KLSG**F**S**F***KKNKK*
dC	*KKKKKR***F**S**F***KKS**F**KLSG**F**S**F***K*
dN	*R***F**S**F***KKS**F**KLSG**F**S**F***KKNKK*
dNdC	*R***F**S**F***KKS**F**KLSG**F**S**F***K*
FA	*KKKKKR*A*A*KKS*A*KLSGA*A*KKNKK*

[a]The italics and bold fonts highlight positively charged and hydrophobic residues, respectively.

In addition to the large number of groups that apparently contribute to binding, a major challenge posed by the MARCKS-ED peptide and its variants is that they are structurally flexible, thus carrying out a sufficient amount of conformational sampling is expected to be essential. For example, two sets of unbinding PMF calculations that start with a fully extended structure give rise to a difference of more than 3 kcal/mol for the estimated binding affinity; both PMF calculations include 80 windows with each window sampled for 10 ns. Although the basic trends in the PMF results shown in Table 4 follow qualitatively that of the experimental data, the PMF data always overestimate the binding affinity, especially for the mutants of MARCKS-ED. As illustrated by the REMD results below, this trend likely reflects that the solution conformations are not sufficiently sampled in the regular PMF calculations.

For the BAR-FEP calculations, we follow the scheme illustrated in Figure 2. More specifically, we first carry out a fairly long (20 ns) equilibrium simulation for the peptide at the membrane surface without any restraints (top right state in Figure 2). Using a representative structure of the membrane-bound ensemble (using clustering analysis) as a reference, we perform (i) one simulation of the peptide on the membrane surface with z coordinate restraint, orientational restraint, and RMSD restraint (bottom right state in Figure 2); (ii) one simulation of the peptide in the aqueous solution with the same sets of restraints (bottom left state in Figure 2); and (iii) also one simulation of the peptide in the aqueous solution without any restraints (top left state in Figure 2). All simulations are 20 ns long; comparison to results with 10 ns of sampling indicates that results do not vary significantly with additional sampling.

To explore the impact of better sampling, we use a temperature based replica exchange MD (REMD) protocol[94] to sample the unrestrained peptides in aqueous solution and on

Table 4. Binding Free Energy (in kcal/mol) of MARCKS-ED Peptides from Experiments and GBSW-GCS-3 Simulations[a]

MARCKS-ED	expt[93]	US[b]	BAR-REMD[c]	BAR-avg[d]	$\langle \Delta\Delta W_{slv} \rangle_{mem}$-REMD[c]	R_g (Å)
WT	−7.8	−10.2 (−9.6)	−7.1 ± 0.9	−7.7 ± 2.6	−13.9 ± 2.6	8.6 ± 0.1
dC	−6.5	−8.6 (−7.9)	−5.1 ± 1.3	−6.2 ± 0.5	−12.2 ± 4.1	8.2 ± 0.2
dN	−5.7	−8.0 (−7.4)	−5.5 ± 1.1	−5.5 ± 2.2	−10.8 ± 3.2	8.0 ± 0.3
dNdC	−5.1	−6.1 (−5.3)	−3.5 ± 1.1	−3.8 ± 2.9	−10.2 ± 4.1	7.3 ± 0.1
FA	−4.6	−8.2 (−7.7)	−4.4 ± 0.6	−3.5 ± 2.5	−9.5 ± 2.6	8.6 ± 0.6

[a]Unscaled PS fraction is 16.7% for all simulations, with a salt concentration 0.1 M of NaCl. [b]The values in parentheses include an estimate of rotational entropy difference between bound and unbound states based on an expression[45] similar to eq 24. [c]The results are based on REMD simulations of 20 ns length for the relevant states; the statistical errors are estimated using block average. [d]The BAR-FEP results (average and standard deviation) are from five to six independent sets of simulations that start from snapshots collected from the REMD simulation (for components, see the Supporting Information).

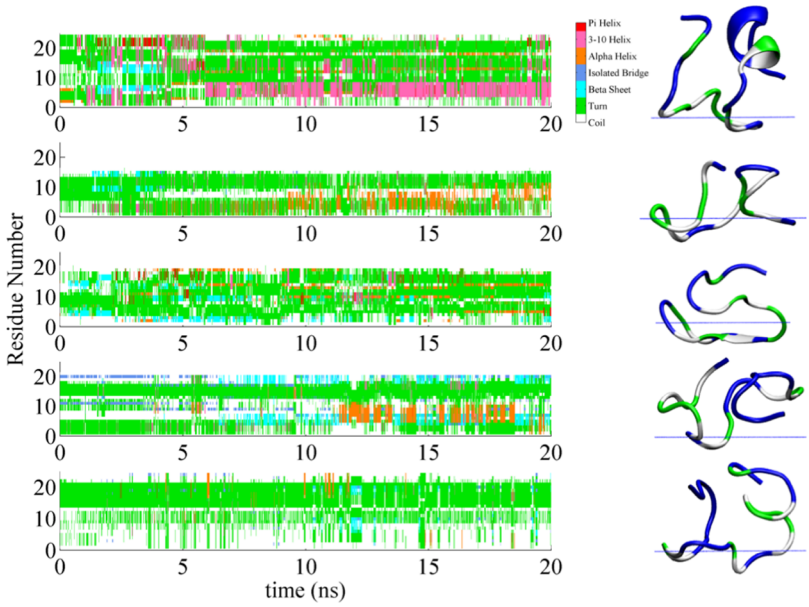

Figure 5. Evolution of secondary structure of the MARCKS-ED peptides during the REMD simulations (results for the 300 K replica are shown); the color coding of the secondary structures is shown on the top panel. On the right, the dominant conformation following a cluster analysis is shown (the blue line indicates the dividing surface in the GBSW-GCS model, i.e., the dashed line in Figure 3); in these structures, green indicates polar residues, blue indicates cationic residues, and white indicates hydrophobic residues. From top to bottom, the sequences are FA, dNdC, dN, dC, and WT (see Table 3).

the membrane surface. In the REMD simulations, temperatures are exponentially spaced for 12 replicas between 300 and 600 K. The exchange rate is maintained around 20% between all adjacent replicas for 2000 exchanges within 20 ns for each replica. We then pick 5−6 dominant bound configurations from the REMD trajectories for each peptide variant using clustering analysis (with 2.0 Å as the RMSD cutoff); using these as references, independent sets of restrained simulations in solution and on the membrane surface are carried out, leading to five to six independent sets of estimated binding affinity for each peptide sequence. The average binding affinities and the corresponding standard deviations are summarized in Table 4; results of individual sets are reported in the Supporting Information. Comparison to results using the first three sets of trajectories indicates that the computed binding free energies no longer vary significantly with additional sampling.

Figure 5 shows the evolution of the secondary structures of the MARCKS-ED peptides during the REMD simulations; the dominant conformation following a clustering analysis is also shown for each sequence, although the RMSD data of the peptides during the simulations (see Supporting Information) suggest that they sample a broad set of structures. All sequences are largely disordered, except for the FA mutant, which is seen to occasionally feature a short 3_{10} helix at the C terminus. These results are qualitatively consistent with the experiment CD spectra for the WT peptide,[95] which indicate a random coil structure. On the other hand, we note that all peptides remain rather compact; the radius of gyration is around 8 Å for all sequences. In previous studies,[43,90,96] the WT MARCKS-ED peptide was interpreted to adopt an extended structure (which would have a $R_g \sim 27.5$ Å) based on CD and EPR data,[95] although our collapsed random coil model is not in conflict with those data.

To characterize the binding mode of the peptides on the membrane surface, the average z value for the center of mass of each residue is shown in Figure 6. For the WT sequence, the

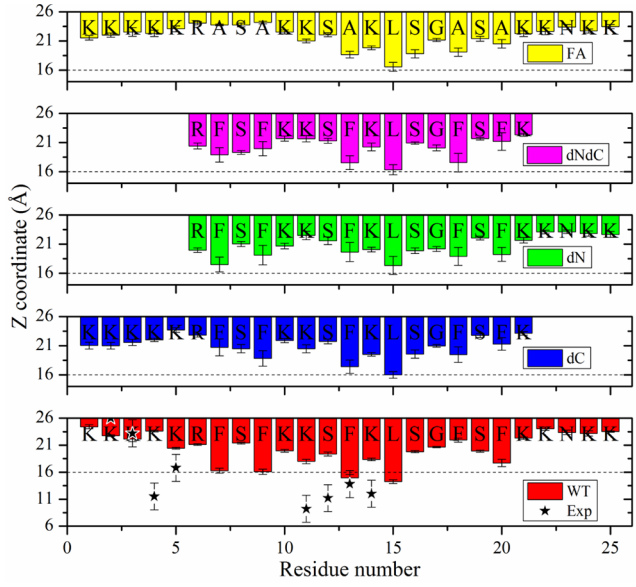

Figure 6. Average z coordinates of amino acid side chains in the MARCKS-ED peptides at a membrane with 16.7% PS and 83.3% PC from GBSW-GCS-3 simulations. For reference, the dielectric interface is at z = 16 Å; thus z < 16 Å indicates insertion into the hydrophobic region of the bilayer. The stars in the WT plot indicate measured values for the nitroxide spin label in EPR studies[95] (see text for Discussions).

hydrophobic residues are generally close to the dielectric boundary (z = 16 Å), while the charged and polar residues remain in the high dielectric constant region. The exception is for the few Lys and Ser residues in the middle segment of the peptide, which remain close to the dielectric interface due to the deep insertion of nearby hydrophobic residues (see Supporting Information for snapshots). On a qualitative scale, the deep insertions of Phe side chains (more than 3 Å below

dx.doi.org/10.1021/ct500218p | J. Chem. Theory Comput. 2014, 10, 2845−2859

the level of phosphate) agree with the EPR measurements,[95,97] NMR experiments,[96,98] and fluorescence correlation spectroscopy measurements.[89] The relatively small variation in the insertion depth for the middle segment is in particular good agreement with the EPR data.[95] The position of the N-terminal Lys_5 segment is observed to be at a distance from the dielectric boundary as well as the level of phosphate groups, also in qualitative agreement with the EPR and NMR data.[95,97,99] At a quantitative level, the EPR data suggested that position 4 is at a similar z position to the middle segment of the peptide, in contrast to our finding. This might be due to the fact that the charge state of the spin-labeled side chain is rather different from a Lys. The C-terminal sequence KKNKK is largely solvated in solution in our MD simulations. Initial EPR data suggested that the C-terminus is at the membrane interface,[95] although this interpretation appeared to have been abandoned since then.[96] For the other peptide variants, the trends in the insertion depth of residues are largely similar to the WT, although on average the peptides are further away from the dielectric interface (Figure 6), which is consistent with their weaker binding affinities, which we turn to next.

As shown in Table 4, the experimental binding affinities of the MARCKS-ED peptides follow largely the magnitude of the net charge, which are +13, +10, +8, and +5 for WT, dC, dN, and dNdC, respectively. The quantitative changes in the magnitude of the binding affinities, however, are smaller than expected based solely on the value of the net charge. For example, while a Lys_5 peptide binds to the same anionic membrane with an affinity of ∼5 kcal/mol (see Table 1), truncation of the N-terminal Lys_5 segment of the MARCKS-ED peptide only leads to a drop of 2.1 kcal/mol in binding free energy. This is not entirely unexpected for a flexible peptide like MARCKS-ED. Figure 6 shows that in the dN mutant, charged residues (especially the C-terminus) are drawn closer to the charged membrane and therefore compensate for the loss of the Lys_5 segment. A similar scenario is observed for the dC mutant, which has a binding affinity only 1.3 kcal/mol lower than the WT, despite the loss of four Lys residues at the C-terminus.

This compensation effect is also seen in the FA mutant, which binds 3.2 kcal/mol weaker to the membrane than the WT; this is about half of the magnitude expected based on the difference in the binding affinity between Phe and Ala, which is 1.3 kcal/mol per residue[100] (there are five Phe to Ala mutations in the FA mutant). Figure 6 shows that Ala inserts significantly shallower than Phe, but the positively charged residues are drawn closer to the anionic membrane. Thus, the loss of hydrophobic insertion is compensated by a more favorable electrostatic contribution, a conclusion also reached in a Monte Carlo study of MARCKS-ED binding using a coarse-grained peptide model.[43]

Regarding the computational results, both (un)binding PMF using umbrella sampling and FEP using BAR give results that are roughly consistent with experimental data. The PMF result did not use REMD simulations, and it is unlikely that the effects associated with conformational heterogeneity and rotational entropy are adequately treated. As a result, the estimated binding affinities are generally further away from the experimental data. We note that these PMF calculations included 800 ns of simulations in total (80 windows and 10 ns per window), highlighting the significant computational expense for this approach. Still, the PMF results without using REMD do not always correlate well with experiments. With the REMD conformational ensembles, the computed binding affinities with the BAR approach are in good agreement with results averaged over five to six sets of independent simulations that start with snapshots taken from the REMD trajectories; moreover, the binding affinities follow the experimental trend rather well. The statistical error in each BAR simulation is small (no more than 0.5 kcal/mol), although there are significant variations in the calculated binding affinity among different sets of simulations, underlining the importance of carrying out adequate conformational sampling for a flexible system like MARCKS-ED. As shown in the Supporting Information, different trajectories may lead to different levels of insertion of hydrophobic residues and packing of these residues. Moreover, the various restraints (z, orientational and RMSD) make notable free energy contributions and may differ significantly among independent simulations, thus highlighting the importance of carefully considering these terms according to Figure 2. Nevertheless, it is encouraging that sensible results can be obtained using the BAR-FEP approach with on the order of 10−20 ns simulation for each relevant state in Figure 2. Finally, we note that for a flexible system like MARCKS-ED, the protocol based on differential solvation PMFs ($\langle \Delta\Delta W_{slv} \rangle_{men}$ in Table 4) leads to a substantial overestimate (by about a factor of 2) of the binding affinity (even after correction of translation/rotational entropy); the relative trends among the peptide variants, however, appear to be adequately captured for this system.

CONCLUDING REMARKS

In this article, we discuss the calculation of binding free energy of proteins/peptides to a charged lipid membrane. This is motivated by the observation that despite the clear importance of protein/peptide binding to charged membranes, most previous computational studies were qualitative in nature and/or focused on short peptides. Establishing an efficient and robust binding free energy protocol that is applicable to both peptides and large proteins can greatly complement experimental studies in identifying physical factors and structural motifs that control the binding affinity and specificity.

Following the discussion of protein/ligand and surface/adsorbate binding calculations, there are two general approaches based on the (un)binding potential of mean force (PMF) and free energy perturbation (FEP). Although application of these approaches with explicit solvent simulations has led to very encouraging results for protein−ligand[49−51] and even protein−protein[56] binding, computation of protein−membrane binding with explicit solvent/membrane simulations following these approaches is computationally expensive and likely encounters serious convergence issues. Therefore, we have set out to explore a method based on an implicit membrane/solvent model (GBSW in combination with the Gouy−Chapman-Stern (GCS) model for a charged interface), which we expect to lead to useful results when the binding does not implicate significant membrane deformation and local demixing of lipids. In fact, by comparing results from an implicit membrane model with those using full atomistic representation of lipids, one is able to gain useful insights regarding the contribution from generic electrostatic effects vs those due to specific protein−lipid interactions. In other words, conducting binding free energy calculations using an implicit membrane/solvent model is not just motivated by computational efficiency, it also leads to novel physical understandings of membrane−protein interactions.

Within the framework of the GBSW-GCS model, we show that the binding free energy can be efficiently computed following a thermodynamic cycle similar to protein/ligand binding calculations, especially when a BAR based protocol is used to consider both the membrane bound and solution conformational ensembles. Test calculations on a series of peptides demonstrate that our computational approach leads to binding affinities in encouraging agreement with experimental data, including for the challenging example of the MARCKS-ED peptides, which are structurally flexible and therefore require extensive conformational sampling using replica exchange molecular dynamics. For more complex applications, it is possible to introduce intermediate states between the membrane bound and solution ensembles as in regular FEP simulations, although we have focused on testing the applicability of the simple two-ensemble protocol; for the peptide systems tested here, it appears that this protocol is effective.

Our development and test calculations also allow us to comment on several technical issues related to binding calculations using an implicit membrane/solvent model. First, for a membrane with a significant fraction of anionic lipids, we emphasize it is essential to include the effect of ion adsorption using the Stern model, which significantly modifies the effective surface charge. Using only the Gouy−Chapman model can lead to a significant overestimation of the binding affinity of highly charged systems. In this context, we found here that setting the charged surface 3 Å away from the dielectric interface appears to lead to more reliable binding affinities, although we note that this is an empirical observation and could be due to the fact that the interfacial dipole potential is not included in our GCS model. Second, we show that the protocol of accumulating differential solvation PMFs over MD simulation for the membrane-bound state can only be useful for rather rigid systems but are not as applicable to flexible systems such as MARCKS-ED. Our BAR based approach considers both the membrane bound and solution conformational ensembles and offers more reliable results. Finally, we reiterate the points made in several previous studies[49−52] that when computing binding free energies and comparing to experimental data, it is important to carefully evaluate all relevant components, such as the rotational entropy difference between bound and unbound states and the definition of standard state.

We focus on relatively simple peptide systems in this study to illustrate our computational methodology. In a separate work, we will report results for a realistic protein (RecA), for which the GBSW-GCS based results are compared to explicit membrane simulations and experimental data. Considering the simplicity of the membrane model, it is encouraging that the results track experimental trends rather well for the systems studied so far. Therefore, it is of interest to apply the methodology to more sophisticated implicit membrane models where effects associated with surface deformation[101,102] and lateral pressure profiles[103−106] are included, so that we can start to systematically evaluate how membrane shape and composition modulate interfacial binding of proteins and peptides at a semiquantitative level. We hope that this work will stimulate additional efforts to develop effective computational methodologies to quantitatively evaluate protein binding to complex membranes. One issue of particular interest, for example, concerns the entropic contribution associated with counterion release, which might be relevant to the binding of highly charged systems to the membrane[18] but is not adequately captured in most implicit solvent/membrane models.

■ ASSOCIATED CONTENT

Supporting Information

Additional results for the binding free energy of selected amino acids to an anionic membrane and the MARCKS-ED peptides are included. This material is available free of charge via the Internet at http://pubs.acs.org/.

■ AUTHOR INFORMATION

Corresponding Author

*E-mail: cui@chem.wisc.edu.

Notes

The authors declare no competing financial interest.

■ ACKNOWLEDGMENTS

The initial development of the research was supported by the NSF grant (NSF-DMS-1160360), and the benchmark/refinement of the methods has been supported by the University of Wisconsin Materials Research Science and Engineering Center (DMR-1121288) through a SEED grant. Computational resources from the Extreme Science and Engineering Discovery Environment (XSEDE), which is supported by NSF grant number OCI-1053575, are greatly appreciated; computations are also supported in part by NSF through a major instrumentation grant (CHE-0840494) to the Chemistry department. We also gratefully acknowledge use of facilities and instrumentation supported by the University of Wisconsin Materials Research Science and Engineering Center (DMR-1121288).

■ REFERENCES

(1) Alberts, B.; Bray, D.; Lewis, J.; Raff, M.; Roberts, K.; Watson, J. D. *Molecular Biology of the Cell*; Garland Publishing, Inc.: New York, 1994.

(2) McLaughlin, S.; Murray, D. Plasma Membrane Phosphoinositide Organization by Protein Electrostatics. *Nature* **2005**, *438*, 605−611.

(3) Rennera, L. D.; Weibel, D. B. Cardiolipin microdomains localize to negatively curved regions of Escherichia coli membranes. *Proc. Natl. Acad. Sci. U. S. A.* **2011**, *108*, 6264−6269.

(4) Groves, J. T.; Kuriyan, J. Molecular mechanisms in signal transduction at the membrane. *Nat. Struct. Mol. Biol.* **2010**, *17*, 659−665.

(5) Phillips, R.; Ursell, T.; Wiggins, P.; Sens, P. Emerging roles for lipids in shaping membrane-protein function. *Nature* **2009**, *459*, 379−385.

(6) Shibata, Y.; Hu, J.; Kozlov, M. M.; Rapoport, T. A. Mechanisms shaping the membranes of cellular organelles. *Annu. Rev. Cell Dev. Biol.* **2009**, *25*, 329−354.

(7) McMahon, H. T.; Gallop, J. L. Membrane curvature and mechanisms of dynamic cell membrane remodeling. *Nature* **2005**, *438*, 590−596.

(8) Bigay, J.; Antonny, B. Curvature, lipid packing, and electrostatics of membrane organelles: defining cellular territories in determining specificity. *Dev. Cell* **2012**, *23*, 886−895.

(9) Brogden, K. A. Antimicrobial peptides: Pore formers or metabolic inhibitors in bacteria? *Nat. Rev. Microbiol.* **2005**, *3*, 238−250.

(10) Epand, R. F.; Mowery, B. P.; Lee, S. E.; Stahl, S. S.; Lehrer, R. I.; Gellman, S. H.; Epand, R. M. Dual mechanism of bacterial lethality for a cationic sequence-random copolymer that mimics host-defense antimicrobial peptides. *J. Mol. Biol.* **2008**, *379*, 38−50.

(11) Schmidt, N. W.; Wong, G. C. L. Antimicrobial Peptides and Induced Membrane Curvature: Geometry, Coordination Chemistry,

and Molecular Engineering. *Curr. Opin. Solid State Mater. Sci.* **2013**, *17*, 151−163.
(12) Cui, Q.; Zhang, L.; Wu, Z.; Yethiraj, A. Generation and sensing of membrane curvature: Where materials science and biophysics meet. *Curr. Opin. Solid State Mater. Sci.* **2013**, *17*, 164−174.
(13) Saludes, J. P.; Morton, L. A.; Ghosh, N.; Beninson, L. A.; Chapman, E. R.; Fleshner, M.; Yin, H. Detection of Highly Curved Membrane Surfaces Using a Cyclic Peptide Derived from Synaptotagmin-I. *ACS Chem. Biol.* **2012**, *7*, 1629−1635.
(14) Morton, L. A.; Yang, H.; Saludes, J. P.; Fiorini, Z.; Beninson, L.; Chapman, E. R.; Fleshner, M.; Xue, D.; Yin, H. MARCKS-ED Peptide as a Curvature and Lipid Sensor. *ACS Chem. Biol.* **2013**, *8*, 218−225.
(15) Neale, C.; Hsu, J. C. Y.; Yip, C. M.; Pomes, R. Indolicidin binding induces thinning of a lipid bilayer. *Biophys. J.* **2014**, *106*, L29−L31.
(16) Vivcharuk, V.; Tomberli, B.; Tolokh, I. S.; Gray, C. G. Prediction of binding free energy for adsorption of antimicrobial peptide lactoferricin B on a POPC membrane. *Phys. Rev. E* **2008**, *77*, 031913.
(17) Tolokh, I. S.; Vivcharuk, V.; Tomberli, B.; Gray, C. G. inding free energy and counterion release for adsorption of the antimicrobial peptide lactoferricin B on a POPG membrane. *Phys. Rev. E* **2009**, *80*, 031911.
(18) Vivcharuk, V.; Kaznessis, Y. Free Energy Profile of the Interaction between a Monomer or a Dimer of Protegrin-1 in a Specific Binding Orientation and a Model Lipid Bilayer. *J. Phys. Chem. B* **2010**, *114*, 2790−2797.
(19) Yeh, I. C.; Ripoll, D. R.; Wallqvist, A. Free Energy Difference in Indolicidin Attraction to Eukaryotic and Prokaryotic Model Cell Membranes. *J. Phys. Chem. B* **2012**, *116*, 3387−3396.
(20) Neale, C.; Bennett, W. F. D.; Tieleman, D. P.; Pomes, R. Statistical Convergence of Equilibrium Properties in Simulations of Molecular Solutes Embedded in Lipid Bilayers. *J. Chem. Theory Comput.* **2011**, *7*, 4175−4188.
(21) Bergstrom, C. L.; Baeles, P. A.; Lv, Y.; Vanderlick, T. K.; Groves, J. T. Cytochrome c causes pore formation in cardiolipin-containing membranes. *Proc. Natl. Acad. Sci. U.S.A.* **2013**, *110*, 6269−6274.
(22) Lai, A. L.; Tamm, L. K.; Ellena, J. F.; Cafiso, D. S. Synaptotagmin 1 Modulates Lipid Acyl Chain Order in Lipid Bilayers by Demixing Phosphatidylserine. *J. Biol. Chem.* **2011**, *286*, 25291−25300.
(23) Ohkubo, Y. Z.; Pogorelov, T. V.; Arcario, M. J.; Christensen, G. A.; Tajkhorshid, E. Accelerating Membrane Insertion of Peripheral Proteins with a Novel Membrane Mimetic Model. *Biophys. J.* **2012**, *102*, 2130−2139.
(24) Baylon, J. L.; Lenov, I. L.; Sligar, S. G.; Tajkhorshid, E. Characterizing the Membrane-Bound State of Cytochrome P450 3A4: Structure, Depth of Insertion, and Orientation. *J. Am. Chem. Soc.* **2013**, *135*, 8542−8551.
(25) Marrink, S. J.; de Vries, A. H.; Tieleman, D. P. Lipids on the move: Simulations of membrane pores, domains, stalks and curves. *Biochim. Biophys. Acta, Biomembr.* **2009**, *1788*, 149−168.
(26) Marrink, S. J.; Tieleman, D. P. Perspective on the Martini model. *Chem. Soc. Rev.* **2013**, *42*, 6801−6822.
(27) Deserno, M. Mesoscopic Membrane Physics: Concepts, Simulations, and Selected Applications. *Macromol. Rapid Commun.* **2009**, *30*, 752−771.
(28) Arkhipov, A.; Yin, Y.; Schulten, K. Four-scale description of membrane sculpting by BAR domains. *Biophys. J.* **2008**, *95*, 2806−2821.
(29) Wu, Z.; Cui, Q.; Yethiraj, A. A New Coarse-grained Force Field for Membrane-peptide Simulations. *J. Chem. Theory Comput.* **2011**, *7*, 3793−3802.
(30) Orsi, M.; Noro, M. G.; Essex, J. W. Dual-resolution molecular dynamics simulation of antimicrobials in biomembranes. *J. R. Soc., Interface* **2011**, *8*, 826−841.
(31) Saunders, M. G.; Voth, G. A. Coarse-graining of multiprotein assemblies. *Curr. Opin. Struct. Biol.* **2012**, *22*, 144−150.
(32) Shinoda, W.; DeVane, R.; Klein, M. L. Computer simulation studies of self-assembling macromolecules. *Curr. Opin. Struct. Biol.* **2012**, *22*, 175−186.
(33) Monticelli, L.; Kandasamy, S. K.; Periole, X.; Larson, R. G.; Tieleman, D. P.; Marrink, S. J. The MARTINI Coarse-Grained Force Field: Extension to Proteins. *J. Chem. Theory Comput.* **2008**, *4*, 819.
(34) Lazaridis, T. Implicit Solvent Simulations of Peptide Interactions With Anionic Lipid Membranes. *Proteins: Struct., Funct., Bioinf.* **2005**, *58*, 518−527.
(35) Im, W.; Feig, M.; Brooks, C. L., III. An Implicit Membrane Generalized Born Theory for the Study of Structure, Stability, and Interactions of Membrane Proteins. *Biophys. J.* **2003**, *85*, 2900−2918.
(36) Chen, J. H.; Brooks, C. L., III; Khandogin, J. Recent advances in implicit solvent-based methods for biomolecular simulations. *Curr. Opin. Struct. Biol.* **2008**, *18*, 140−148.
(37) Khelashvili, G.; Harries, D.; Weinstein, H. Modeling Membrane Deformations and Lipid Demixing upon Protein-Membrane Interaction: The BAR Dimer Adsorption. *Biophys. J.* **2009**, *97*, 1626−1635.
(38) Mondal, S.; Khelashvili, G.; Shan, J. F.; Andersen, O. S.; Weinstein, H. Quantitative Modeling of Membrane Deformations by Multihelical Membrane Proteins: Application to G-Protein Coupled Receptors. *Biophys. J.* **2011**, *101*, 2902−2101.
(39) Im, W.; Brooks, C. L., III. Interfacial folding and membrane insertion of designed peptides studied by molecular dynamics simulations. *Proc. Natl. Acad. Sci. U.S.A.* **2005**, *102*, 6771−6776.
(40) Mihajlovic, M.; Lazaridis, T. Antimicrobial peptides bind more strongly to membrane pores. *Biochim. Biophys. Acta, Biomembr.* **2010**, *1798*, 1494−1502.
(41) He, Y.; Prieto, L.; Lazaridis, T. Modeling peptide binding to anionic membrane pores. *J. Comput. Chem.* **2013**, *34*, 1463−1475.
(42) He, Y.; Lazaridis, T. Activity Determinants of Helical Antimicrobial Peptides: A Large-Scale Computational Study. *PLoS One* **2013**, *8*, e66440.
(43) Tzlil, S.; Murray, D.; Ben-Shaul, A. The "Electrostatic-Switch" Mechanism: Monte Carlo Study of MARCKS-Membrane Interaction. *Biophys. J.* **2008**, *95*, 1745−1757.
(44) Ben-Tal, N.; Honig, B.; Miller, C.; McLaughlin, S. Electrostatic binding of proteins to membranes. Theoretical predictions and experimental results with charybdotoxin and phospholipid vesicles. *Biophys. J.* **1997**, *73*, 1717−1727.
(45) Ben-Tal, N.; Honig, B.; Bagdassarian, C. K.; Ben-Shaul, A. Association Entropy in Adsorption Processes. *Biophys. J.* **2000**, *79*, 1180−1187.
(46) Bechor, D.; Ben-Tal, N. Implicit Solvent Model Studies of the Interactions of the Influenza Hemagglutinin Fusion Peptide with Lipid Bilayers. *Biophys. J.* **2001**, *80*, 643−655.
(47) Shental-Bechor, D.; Haliloglu, T.; Ben-Tal, N. Interactions of Cationic-Hydrophobic Peptides with Lipid Bilayers: A Monte Carlo Simulation Method. *Biophys. J.* **2007**, *93*, 1858−1871.
(48) Mihajlovic, M.; Lazaridis, T. Calculations of pH-dependent binding of proteins to biological membranes. *J. Phys. Chem. B* **2006**, *110*, 3375−3384.
(49) Wang, J.; Deng, Y.; Roux, B. Absolute Binding Free Energy Calculations Using Molecular Dynamics Simulations with Restraining Potentials. *Biophys. J.* **2006**, *91*, 2798−2814.
(50) Deng, Y.; Roux, B. Calculation of Standard Binding Free Energies: Aromatic Molecules in the T4 Lysozyme L99A Mutant. *J. Chem. Theory Comput.* **2006**, *2*, 1255−1273.
(51) Gumbart, J. C.; Roux, B.; Chipot, C. Standard Binding Free Energies from Computer Simulations: What Is the Best Strategy? *J. Chem. Theory Comput.* **2013**, *9*, 794−802.
(52) Mori, T.; Hamers, R. J.; Pedersen, J. A.; Cui, Q. An Explicit Consideration of Desolvation is Critical to Binding Free Energy Calculations of Charged Molecules at Ionic Surfaces. *J. Chem. Theory Comput.* **2013**, *9*, 5059−5069.
(53) Bennett, C. H. Efficient Estimation of Free Energy Difference from Monte Carlo Data. *J. Comput. Phys.* **1976**, *22*, 245−268.
(54) Pohorille, A.; Jarzynski, C.; Chipot, C. Good Practices in Free-Energy Calculations. *J. Phys. Chem. B* **2010**, *114*, 10235−10253.

(55) Grossfield, A. WHAM: an implementation of the weighted histogram analysis method, version 2.0.7. http://membrane.urmc.rochester.edu/content/wham/.
(56) Gumbart, J. C.; Roux, B.; Chipot, C. Efficient Determination of Protein-Protein Standard Binding Free Energies from First Principles. *J. Chem. Theory Comput.* **2013**, *9*, 3789−3798.
(57) Roux, B.; Simonson, T. Implicit solvent models. *Biophys. Chem.* **1999**, *78*, 1−20.
(58) Ovchinnikov, V.; Cecchini, M.; Karplus, M. A Simplified Confinement Method for Calculating Absolute Free Energies and Free Energy and Entropy Differences. *J. Phys. Chem. B* **2013**, *117*, 750−762.
(59) Tzlil, S.; Ben-Shaul, A. Flexible Charged Macromolecules on Mixed Fluid Lipid Membranes: Theory and Monte Carlo Simulations. *Biophys. J.* **2005**, *89*, 2972−2987.
(60) Lazaridis, T.; He, Y.; Prieto, L. Membrane Interactions and Pore Formation by the Antimicrobial Peptide Protegrin. *Biophys. J.* **2013**, *104*, 633−642.
(61) McQuarrie, D. A. *Statistical Mechanics*; Harper and Row: New York, 1973.
(62) Frenkel, D.; Smit, B. *Understanding Molecular Simulation: From Algorithms to Applications*; Academic Press: San Diego, CA, 2002.
(63) Zuckerman, D. M.; Woolf, T. B. Theory of a Systematic Computational Error in Free Energy Differences. *Phys. Rev. Lett.* **2002**, *89*, 180602.
(64) Bruckner, S.; Boresch, S. Efficiency of Alchemical Free Energy Simulations. I. A practical Comparison of the Exponential Formula, Thermodynamic Integration, and Bennett's Acceptance Ratio Method. *J. Comput. Chem.* **2011**, *32*, 1303−1319.
(65) Herschbach, D. R.; Johnston, H. S.; Rapp, D. Molecular Partition functions in terms of local properties. *J. Chem. Phys.* **1959**, *31*, 1652−1661.
(66) Boresch, S.; Tettinger, F.; Leitgeb, M.; Karplus, M. Absolute Binding Free Energies: A Quantitative Approach for Their Calculation. *J. Phys. Chem. B* **2003**, *107*, 9535−9551.
(67) Im, W.; Lee, M. S.; Brooks, C. L., III. Generalized Born Model with a Simple Smoothing Function. *J. Comput. Chem.* **2003**, *24*, 1691−1702.
(68) Formaneck, M. S.; Cui, Q. The Use of a Generalized Born Model for the Analysis of Protein Conformational Transitions: A Comparative Study with Explicit Solvent Simulations for Chemotaxis Y Protein (CheY). *J. Comput. Chem.* **2006**, *27*, 1923−1943.
(69) Yuzlenko, O.; Lazaridis, T. Membrane Protein Native State Discrimination by Implicit Membrane Models. *J. Comput. Chem.* **2013**, *34*, 731−738.
(70) Chen, J.; Im, W.; Brooks, C. L., III. Refinement of NMR structures using implicit solvent and advanced sampling techniques. *J. Am. Chem. Soc.* **2004**, *126*, 16038−47.
(71) Chen, J.; Im, W.; Brooks, C. L., III. Balancing solvation and intramolecular interactions: toward a consistent generalized Born force field. *J. Am. Chem. Soc.* **2006**, *128*, 3728−36.
(72) Barrat, J. L.; Hansen, J.-P. *Basic Concepts for simple and complex liquids*; Cambridge University Press: Cambridge, U. K., 2003.
(73) Grahame, D. C. The Electrical Double Layer and the Theory of Electrocapillarity. *Chem. Rev.* **1947**, *41*, 441−501.
(74) Harder, E.; MacKerell, A. D.; Roux, B. Many-body polarization effects and the membrane dipole potential. *J. Am. Chem. Soc.* **2009**, *131*, 2760−2761.
(75) Zhan, H.; Lazaridis, T. Influence of the membrane dipole potential on peptide binding to lipid bilayers. *Biophys. Chem.* **2012**, *161*, 1−7.
(76) Wu, Z. The importance of water electrostatic interactions: new coarse-grained force field development and its applications. Ph.D. thesis, University of Wisconsin—Madison, Madison, WI, 2012.
(77) Stern, O. Zur theorie der elektrolytischen doppelschicht. *Z. Elektrochem.* **1924**, *30*, 508−516.
(78) Eisenberg, M.; Gresalfi, T.; Riccio, T.; McLaughlin, S. Adsorption of Monovalent Cations to Bilayer Membranes Containing Negative Phospholipidst. *Biochemistry* **1979**, *18*, 5213.
(79) McDaniel, R. V.; Sharp, K.; Brooks, D.; McLaughlin, A. C.; Winiski, A. P.; Cafiso, D.; McLaughlin, S. Electrokinetic and Electrostatic Properties of Bilayers Containing Gangliosides G_{M1}, G_{D1a} or G_{T1}. Comparison with a Nonlinear Theory. *Biophys. J.* **1986**, *49*, 741−752.
(80) Ben-Tal, N.; Honig, B.; Peitzsch, R. M.; Denisov, G.; McLaughlin, S. Binding of Small Basic Peptides to Membranes Containing Acidic Lipids: Theoretical Models and Experimental Results. *Biophys. J.* **1996**, *71*, 561−575.
(81) Hartsel, S. C.; Cafiso, D. S. A test of discreteness-of-charge effects in phospholipid vesicles: measurements using paramagnetic amphiphiles. *Biochemistry* **1986**, *25*, 8214−8219.
(82) Langner, M.; Cafiso, D.; Marcelja, S.; McLaughlin, S. Electrostatics of phosphoinositide bilayer membranes Theoretical and experimental results. *Biophys. J.* **1990**, *57*, 335−349.
(83) Winiski, A. P.; McLaughlin, A. C.; McDaniel, R. V.; Eisenberg, M.; McLaughlin, S. An experimental test of the discreteness-of-charge effect in positive and negative lipid bilayers. *Biochemistry* **1986**, *25*, 8206−8214.
(84) Kim, J.; Mosior, M.; Chung, L. A.; Wu, H.; McLaughlin, S. Binding of peptides with basic residues to membranes containing acidic phospholipids. *Biophys. J.* **1991**, *60*, 135−148.
(85) Shirts, M. R.; Mobley, D. L. An Introduction to Best Practices in Free Energy Calculations. *Methods Mol. Biol.* **2013**, *924*, 271−311.
(86) Lee, S.; Mihara, H.; Aoyagi, H.; Kato, T.; Izumiya, N.; Yamasaki, N. Relationship between antimicrobial activity and amphiphilic property of basic model peptides. *Biochim. Biophys. Acta, Biomembr.* **1986**, *862*, 211−219.
(87) Taniguchi, H.; Manenti, S. Interaction of myristoylated alanine-rich protein kinase C substrate (MARCKS) with membrane phospholipids. *J. Biol. Chem.* **1993**, *268*, 9960−9963.
(88) Kim, J.; Shishido, T.; Jiang, X.; Aderem, A.; McLaughlin, S. Phosphorylation, high ionic strength, and calmodulin reverse the binding of MARCKS to phospholipid vesicles. *J. Biol. Chem.* **1994**, *269*, 28214−28219.
(89) Rusu, L.; Gambhir, A.; McLaughlin, S.; Rädler, J. Fluorescence Correlation Spectroscopy Studies of Peptide and Protein Binding to Phospholipid Vesicles. *Biophys. J.* **2004**, *87*, 1044−1053.
(90) Gambhir, A.; Hangyás-Mihályné, G.; Zaitseva, I.; Cafiso, D. S.; Wang, J.; Murray, D.; Pentyala, S. N.; Smith, S. O.; McLaughlin, S. Electrostatic sequestration of PIP2 on phospholipid membranes by basic/aromatic regions of proteins. *Biophys. J.* **2004**, *86*, 2188−2207.
(91) Sundaram, M.; Cook, H. W.; Byers, D. M. The MARCKS family of phospholipid binding proteins: regulation of phospholipase D and other cellular components. *Biochem. Cell. Biol.* **2004**, *82*, 191−200.
(92) Dietrich, U.; Krüger, P.; Gutberlet, T.; Käs, J. A. Interaction of the MARCKS peptide with PIP_2 in phospholipid monolayers. *Biochim. Biophys. Acta, Biomembr.* **2009**, *1788*, 1474−1481.
(93) Wang, J.; Gambhir, A.; Hangyás-Mihályné, G.; Murray, D.; Golebiewska, U.; McLaughlin, S. Lateral Sequestration of Phosphatidylinositol 4,5-Bisphosphate by the Basic Effector Domain of Myristoylated Alanine-rich C Kinase Substrate Is Due to Nonspecific Electrostatic Interactions. *J. Biol. Chem.* **2002**, *277*, 34401−34412.
(94) Sugita, Y.; Okamoto, Y. Replica-exchange molecular dynamics method for protein folding. *Chem. Phys. Lett.* **1999**, *314*, 141−151.
(95) Qin, Z.; Cafiso, D. S. Membrane Structure of Protein Kinase C and Calmodulin Binding Domain of Myristoylated Alanine Rich C Kinase Substrate Determined by Site-Directed Spin Labeling. *Biochemistry* **1996**, *35*, 2917−2925.
(96) Ellena, J. F.; Burnitz, M. C.; Cafiso, D. S. Location of the Myristoylated Alanine-Rich C-Kinase Substrate (MARCKS) Effector Domain in Negatively Charged Phospholipid Bicelles. *Biophys. J.* **2003**, *85*, 2442−2448.
(97) Victor, K.; Jacob, J.; Cafiso, D. S. Interactions Controlling the Membrane Binding of Basic Protein Domains: Phenylalanine and the Attachment of the Myristoylated Alanine-Rich C-Kinase Substrate Protein to Interfaces. *Biochemistry* **1999**, *38*, 12527.

(98) Zhang, W.; Crocker, E.; McLaughlin, S.; Smith, S. O. Binding of Peptides with Basic and Aromatic Residues to Bilayer Membranes. *J. Biol. Chem.* **2003**, *278*, 21459−21466.
(99) Victor, K. G.; Cafiso, D. S. Location and dynamics of basic peptides at the membrane interface: EPR of TOAC-labeled peptides. *Biophys. J.* **2001**, *81*, 2241−2250.
(100) Wimley, W. C.; White, S. H. Experimentally determined hydrophobicity scale for proteins at membrane interfaces. *Nat. Struct. Biol.* **1996**, *3*, 842−848.
(101) Choe, S.; Hecht, K. A.; Grabe, M. A Continuum Method for Determining Membrane Protein Insertion Energies and the Problem of Charged Residues. *J. Gen. Physiol.* **2008**, *131*, 563−573.
(102) Panahi, A.; Feig, M. Dynamic Heterogeneous Dielectric Generalized Born (DHDGB): An Implicit Membrane Model with a Dynamically Varying Bilayer Thickness. *J. Chem. Theory Comput.* **2013**, *9*, 1709−1719.
(103) Ollila, O. H. S.; Risselada, H. J.; Louhivuori, M.; Lindahl, E.; Vattulainen, I.; Marrink, S. J. 3D Pressure Field in Lipid Membranes and Membrane-Protein Complexes. *Phys. Rev. Lett.* **2009**, *102*, 078101.
(104) Yoo, J.; Cui, Q. Curvature generation and pressure profile modulation in membrane by lysolipids: insights from coarse-grained simulations. *Biophys. J.* **2009**, *97*, 2267−76.
(105) Yoo, J.; Cui, Q. Three-dimensional stress field around a membrane protein: atomistic and coarse-grained simulation analysis of gramicidin A. *Biophys. J.* **2013**, *104*, 117−127.
(106) Zhan, H.; Lazaridis, T. Inclusion of Lateral Pressure/Curvature Stress Effects in Implicit Membrane Models. *Biophys. J.* **2013**, *104*, 643−654.